APPLIED PHYSICS LETTERS **104**, 041111 (2014)

# A high carrier injection terahertz quantum cascade laser based on indirectly pumped scheme

S. G. Razavipour,[1,a)] E. Dupont,[2] C. W. I. Chan,[3] C. Xu,[1] Z. R. Wasilewski,[1] S. R. Laframboise,[2] Q. Hu,[3] and D. Ban[1]

[1]*Department of Electrical and Computer Engineering, Waterloo Institute for Nanotechnology, University of Waterloo, 200 University Ave. W., Waterloo, Ontario N2L3G1, Canada*
[2]*National Research Council, Blg. M-50, 1200 Montreal Rd., Ottawa, Ontario K1A0R6, Canada*
[3]*Department of Electrical Engineering and Computer Science, Research Laboratory of Electronics, Massachusetts Institute of Technology, Cambridge, Massachusetts 02139, USA*

(Received 31 August 2013; accepted 1 January 2014; published online 29 January 2014)

A Terahertz quantum cascade laser with a rather high injection coupling strength based on an indirectly pumped scheme is designed and experimentally implemented. To effectively suppress leakage current, the chosen quantum cascade module of the device is based on a five-well $GaAs/Al_{0.25}Ga_{0.75}As$ structure. The device lases up to 151 K with a lasing frequency of 2.67 THz. This study shows that the effect of higher energy states in carrier transport and the long-range tunnel coupling between states that belong to non-neighbouring modules have to be considered in quantum design of structures with a narrow injector barrier. Moreover, the effect of interface roughness scattering between the lasing states on threshold current is crucial. © *2014 AIP Publishing LLC*. [http://dx.doi.org/10.1063/1.4862177]

Since the invention of Terahertz (THz) quantum cascade lasers (QCLs),[1] different structure schemes were presented to improve their temperature performance, attempting to achieve lasing operation at thermo-electric cooling temperatures. Even though the limitations of resonant tunneling (RT) structures were noticed by many researchers,[2–5] most of high performance THz QCLs were based on this RT scheme and a $GaAs/Al_{0.15}Ga_{0.85}As$ material system.[6–9] Recently an indirectly pumped (IDP) structure, formerly demonstrated in mid-infrared QCLs,[10] started to be implemented in THz QCLs in the hope of improving device temperature performance. So far, two different types of IDP structures were demonstrated. Kumar *et al.*[4] and Fujita *et al.*[11] reported a four-well and five-well IDP structure with a high coupling strength injection and RT extraction followed by phonon scattering, while Dupont *et al.* demonstrated an IDP structure, named phonon-photon-phonon (3P), with a low injection coupling strength and a direct phonon relaxation mechanism without tunneling.[5,12] In the latter design, the injection coupling strength was sacrificed in order to minimize early negative differential resistance (NDR) prior to lasing threshold. In this paper, we present a 3P design structure with a rather high coupling strength injection and a five-well quantum cascade module, focusing on achieving high output power and high temperature operation. For this purpose, a narrow injector barrier is chosen to enhance lasing dynamic range. In addition, an extra well is included in the upper phonon stream to, on the one hand, reduce the intermediate resonance before the threshold and, on the other hand, minimize the rate of wrong injection by scattering to the lower lasing state (LLS), and thus, increase device internal quantum efficiency. A similar approach was adopted in a low frequency (1.9 THz) RT-QCL.[13]

Similar to what was presented in Ref. 5 and recently in Ref. 12, the first four states of this five-well 3P-QCL play the most important role in carrier transport and lasing operation. Nevertheless, the effect of the fifth and sixth energy states cannot be ignored because of the narrow injector barrier in this new design.[12] As a result, a simplified rate equation (RE) model that includes the first six states of one cascade module was employed to predict the behavior of this laser.

Figure 1 shows the conduction band and moduli wavefunctions of the quantum states of the design which is based on $GaAs/Al_{0.25}Ga_{0.75}As$ material system. The first three wells after the injector barrier form the named upper phonon stream, and the next two wells form the lower phonon stream. The inclusion of one extra well in upper phonon stream helps us to engineer the wavefunctions of levels $i$ (injector state) and $2$ (upper lasing state (ULS)) with more freedom. This results in a fast (and desired) injection from level $i$ to level $2$ (0.3 ps at 10 K) and a slow wrong injection rate (4.65 ps at 10 K) from level $i$ to the level $1$ LLS. Since the energy spacing between levels $2$ and $e$ (extraction state, which alone forms a one-state injector region to pump the next module) is 46.7 meV (only 10 meV higher than the phonon energy in GaAs material), the wrong extraction ($2 \rightarrow e$) rate has to be minimized by lowering the wavefunction overlap between those states. Using a relatively thick radiative barrier serves this purpose while the oscillator strength is also lowered and the population inversion at high temperatures may thus be improved.

All reported devices based on the 3P scheme (V843 (Ref. 5) and V845 (Ref. 12)) were suffering from a thick injector barrier which impedes carrier injection from level $e$ to $i$. Carriers were accumulated in level $e$ and the device performance was deteriorated due to backfilling from level $e$ to $1$. Simulation at 10 K and $e$-$i$ resonance shows that the relative carrier population at level $e$ was 37% in V843 and 42% in V845. A thin injector barrier in this structure results in a high coupling strength injection ($\hbar\Omega_{ei} = 1.54$ meV) which is

a)Electronic mail: sgrazavi@uwaterloo.ca.

 © 2014 AIP Publishing LLC

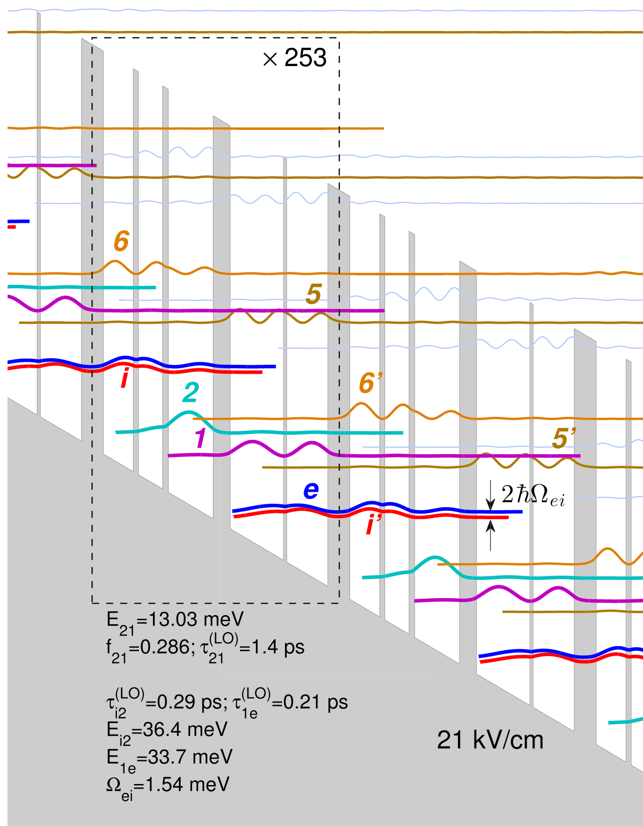


FIG. 1. Conduction band diagram and the moduli squared of wavefunctions of a THz 3P-QCL at 21 kV/cm. The quantum structure, starting with an injector barrier, is **35**/48/**8**/38.9/**9**/72/**27**/85.6/**5**/66 Å, where the bold font indicates the barrier. The center 20 Å of the 48 Å first well after the injector barrier is doped with Si to $1.5 \times 10^{17}$ cm$^{-3}$ to give a two-dimensional carrier concentration of $3 \times 10^{10}$ cm$^{-2}$ per module. The intersubband lifetimes through LO phonon emission are given at the resonant in-plane kinetic energy.

higher than those of V843 ($\hbar\Omega_{ei}$ = 1.14 meV) and V845 ($\hbar\Omega_{ei}$ = 0.85 meV) while it employs a one-state injector region. This structure has a slightly lower coupling strength injection compared to the structure presented by Fujita *et al.* (2 meV),[11] which is based on two-state injector region. In addition, the injection efficiency ($\frac{\tau_{i1}}{\tau_{i1}+\tau_{i2}}$) of previous 3P structures was not high. Adding one extra well in upstream phonon wells allowed us to easily engineer the wavefunction so that the injection efficiency improved from 0.86 in V843 and 0.85 in V845 to 0.94 in this structure at 10 K. Moreover, the three-well structure of the upper phonon stream allows us to minimize the wrong coupling strengths $\Omega_{e1}$ and $\Omega_{e2}$ (at their resonance) while designing a rather high $\Omega_{ei}$.

The five-well 3P structure consists of 253 repeats of this module and is grown at NRC on a semi-insulating (SI) GaAs substrate by molecular beam epitaxy (MBE) with a total thickness of 10 $\mu$m. The active region is sandwiched between a 100 nm of $3 \times 10^{18}$ cm$^{-3}$ bottom n$^+$ GaAs and a top stack of 40 nm of $7 \times 10^{17}$ cm$^{-3}$, 50 nm of $5 \times 10^{18}$ cm$^{-3}$, 10 nm of $5 \times 10^{19}$ cm$^{-3}$ n$^+$, and 3.5 nm of low-temperature grown GaAs.

Two different fabrication processes were employed. Device A has a Au–Au ridge waveguide with a 144 $\mu$m width and 831 $\mu$m length while device B has a 159 $\mu$m width and 1.87 mm length. In addition, the 100 nm thick top contact layer of device B was removed to lower the waveguide loss. The fabrication process and the characterization set-up are the same as what were used for both V843 and V845 to ensure fair comparison. Figure 2 shows the pulsed light–current density–voltage (L–J–V) characteristics of device A from 9 K to 144 K, with a pulse duration of 250 ns and repetition rate of 1 kHz. A threshold current density of 1.44 kA/cm$^2$ was measured at 9 K, while the maximum current density was 2.06 kA/cm$^2$. The L–J characteristics display a roll-over in optical power (confirmed with other devices), a phenomenon that was not observed in previously reported 3P-QCLs.[5,12] The issue of roll-over in THz IDP-QCLs has been explained by the excess energy of carriers in the injector region (voltage drop per module $-2\ E_{LO}$, which equals here 9.5 meV at 21 kV/cm) in combination with a rather high injection coupling.[11,14] More work is required to confirm, if this explanation applies, or not, to our structure.

A clear slope change in V–J curves at threshold can be observed from 9 K to 130 K of the lasing device, reflecting the improved efficiency of this design compared to previous THz 3P-QCLs. The relative change in the measured differential resistance of V962 ($\Delta R_{th}/R_{th} = 33\%$ at 9 K) is higher than those of V845 ($\sim$16%) and V843 (experimentally imperceptible), which results in a higher output emission power. This is because the laser dynamic range (in current) and, consequently, the output optical power are directly related to $\Delta R_{th}/R_{th}$. This improved discontinuity could be a signature of a minimized wrong extraction from ULS to level $e$,[5] which in turn should increase the internal quantum efficiency.

The collected optical power is more than twice of what was collected in V845 with the same set-up and four times higher than that of V843. The maximum operating temperature was improved from 128.5 K in V845 and 138 K in V843 to 144 K (this five-well device) with the same waveguide process. The maximum operating temperature of this device is 151 K which belongs to device B due to a lower

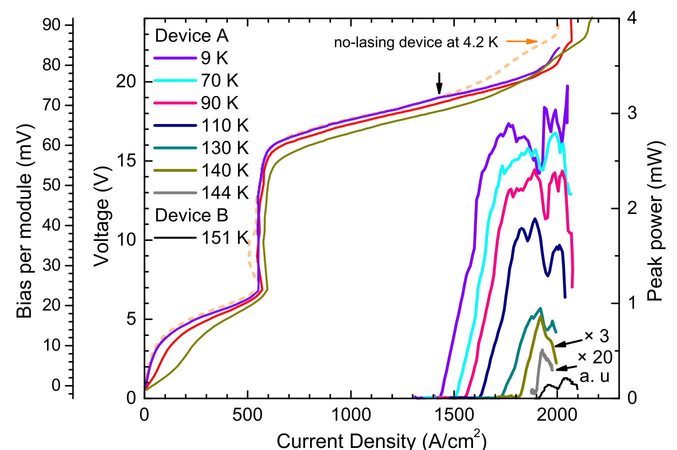


FIG. 2. Left axis: The bias voltage of five-well THz 3 P-QCL (V962) with a Au–Au ridge waveguide with a 144 $\mu$m width and 831 $\mu$m length versus the current density of the lasing device (solid lines) at 9 K, 90 K, and 140 K. In addition, the J–V curve of a rectangle mesa (non-lasing device) at 4.2 K with 0.8 V vertical shift is plotted in dashed line. The short vertical black arrow shows the change in the slope of the V–J curves at laser threshold. The most left vertical axis represents the bias per cascade module on the Au–Au waveguide devices and accounts for the Schottky drop voltage of the top contact. Right axis: Collected THz light (optical output power) versus current density of device A (9 K to 144 K) and device B (151 K).

waveguide loss. The first NDR of both the non-lasing (orange dashed line) and the lasing device (purple line) is observed at 7.1 V while the final NDR is at different biases (22.8 V for non-lasing and 22.0 V for lasing). Even though the maximum current density of the structure is as expected high due to the narrow injector barrier, the intermediate tunneling current ($J_{res} = 575\,\mathrm{A/cm^2}$) is not as low as what we initially expected; the inclusion of one extra well in upper phonon stream is supposed to adequately minimize the intermediate tunneling current.

To understand the experimental observations in this structure, a simplified RE model that includes all six lowest states in each module is employed. All calculation assumptions are the same as what were used in Ref. 12, except the electron temperature of the injection state. Since a recent micro-photoluminescence experiment shows that the difference between the electron temperature ($T_e$) and the lattice temperature ($T_L$) for the injection state is higher than that of other states,[15] we choose $\Delta T$ ($T_e - T_L$) of 100 K for the injection state while $\Delta T = 50$ K for all other subbands.

Figure 3(a) shows the calculated current density-electric field curves, based on the second-order tunneling model, for lasing (red) and non-lasing (black) devices. Experimental curves are also shown in the figure for comparison; they account for the Schottky drop voltage (0.8 V) of the top contact. Except the first resonance current density, the non-lasing current simulation is nicely matched with the experimental results. A small shoulder at 19.5 kV/cm, observed in both simulation and experimental results, is attributed to the combination of two different leakage paths. The first leakage path, shown in black dashed curve in Fig. 3(b), comes from tunneling between levels $2_n$ (ULS of the left module) and $6_{n+1}$ (sixth state of the right module) due to high coupling strength between the wavefunctions of those states ($\Omega_{26} = 1$ meV at 19.5 kV/cm). This *2–6* tunnel channel was an oversight at design stage before MBE growth. The current path between those states starts to be dominant at 19.5 kV/cm, even though the detuning energy between those levels is large ($\Delta_{26} = 12.2$ meV at 19.5 kV/cm). In the non-lasing device, since the carrier relaxation from levels *2* to *1* due to stimulated emission is not relevant and the non-lasing scattering time is relatively long, even a small tunneling rate could be a reason of a leakage. As a result, carriers that are piled up in the ULS could tunnel to the level *6* of the next module ($6_{n+1}$) at electric field of 19.5 kV/cm and beyond, leading to the increase in current. The second leakage path which comes from tunneling between levels $1_n$ (LLS of the left module) and $5_{n+1}$ is not dominant since the carrier population of level *1* is not large due to fast relaxation time from level *1* to level *e*. This current, plotted in orange dashed line in Fig. 3(b), shows a peak at 19.5 kV/cm where those states are aligned. The final NDR of the non-lasing device is revealed at 22 kV/cm, both experimentally and theoretically (Fig. 3). The *e-i* current path (blue curve in Fig. 3(b)) has the main contribution in total current density of the device after 15 kV/cm, while by adding *2–6* leakage path (red curve in Fig. 3(b)) and also *1–5* leakage path (green curve in Fig. 3(b)), the total current density can be fairly predicted with a shoulder at around 19.5 kV/cm. The story is different in lasing devices where stimulated emission

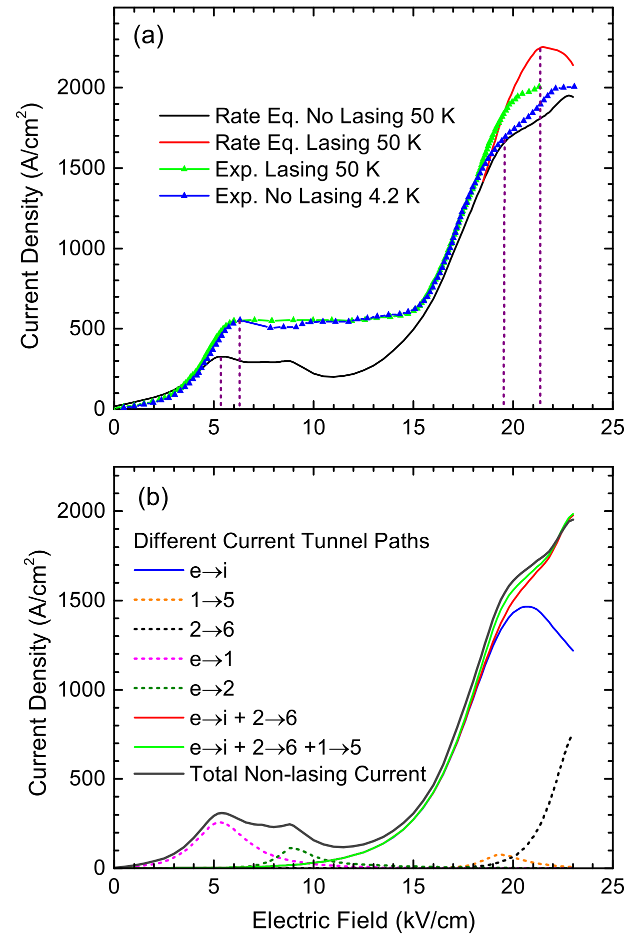


FIG. 3. (a) The current density vs. electric field was calculated by using a RE formalism and second-order tunneling method at 50 K for lasing (red) and non-lasing (black) devices. The experimental curve of nonlasing (at 4.2 K) and lasing (at 50 K) device are shown in dotted lines for comparison. The vertical dashed lines represent the electric fields of the first NDR, final NDR, and shoulder in IV curve. The Loss × FWHM product of 38 THz cm$^{-1}$ was used during this simulation (see Ref. 12). (b) Different simulated current paths of the nonlasing device at 50 K. The four dashed lines show the leakage currents from different tunnel paths. The blue solid curve shows the current path from level *e* to *i*. Combination of different paths are also plotted in colored solid curves to show how they affect the total current (solid black curve) of the device.

become the dominant relaxation mechanism between the lasing levels. Since the stimulated emission reduces the relaxation time of level *2*, the carriers on that level have less chance of tunneling to level $6_{n+1}$; then the current leakage path from ULS to level $6_{n+1}$ is less effective but will impede laser operation at high temperature. In addition, due to gain clamping, the population of level *2* does not increase as rapidly with electric field above threshold, resulting in a lower *2–6* leakage current than in the non-lasing case. The maximum current density in both simulation and experiment occurs at 21.2 kV/cm, the final NDR electrical field, as shown in Fig. 3(a).

There is a noticeable discrepancy between our calculation and experiment in the prediction of the intermediate resonant current and voltage. The first NDR of this device occurs at 7.1 V, which corresponds to an electric field of 6.3 kV/cm (7.1 − 0.8 V, Schottky drop voltage). The measured current density of the device at that electric field is 575 A/cm$^2$. The RE modeling shows the alignment between the levels $e_{n-1}$ and $1_n$ should occur at 5.1 kV/cm with a

coupling strength of $\hbar\Omega_{e1} = 0.32$ meV and a tunneling current density of 340 A/cm$^2$ (pink dashed line in Fig. 3(b)), which is almost half of the measured value. Since the injector barrier of this structure is thin, there is a possibility of injecting carriers directly to a state of a non-neighboring module. Our calculation shows that level $e_{n-1}$ will be in resonance with level $i_{n+1}$ at 6.4 kV/cm, roughly agreeing with the measured resonance electric field (6.3 kV/cm). Figure 4 shows the conduction band diagram of the THz 3P-QCL at electric field of 6.4 kV/cm. An extra leakage current may result from the coupling between the states $e_{n-1}$ and $i_{n+1}$, which occurs right after the alignment of states $e_{n-1}$ and $1_n$ (5.1 kV/cm) and before the alignment of states $e_{n-1}$ and $2_n$ (9 kV/cm). Preliminary simulation based on Dinh's density matrix model[16] shows that the contribution of this channel is not negligible and can explain the first NDR at 6.3 kV/cm.

Our simulation indicates that the improvement in current dynamic range of 3P-QCLs is not trivial. Even though the combination of an extra well in upper phonon wells and a narrow injector barrier increases the maximum current density of the device while keeping the intermediate resonance current lower than the threshold current, we did not have a good control in threshold current density. The scattering time between lasing states of V962 is almost the same as that of V845 at different electric fields, and it is mostly limited by interface roughness (IR) scattering between those states (e.g., $\tau_{21} = 1.8$ ps and $\tau_{21}^{\mathrm{IR}} = 2.7$ ps in both V845 and V962 at 18.5 kV/cm and $T_L = 50$ K).[17] Therefore, the voltage dependence of the effective lifetime (which relates population inversion and pumping rate) is mainly explained by $\tau_{21}^{\mathrm{IR}}$. Since both structures have almost the same oscillator strength and lasing frequency (especially around threshold) and therefore, presumably the same waveguide loss, comparing the threshold current densities is approximately equivalent to comparing the effective lifetimes. At the threshold electric field (18.2 kV/cm in V962 and 19.4 kV/cm in V845[18]) and low temperature, the computed effective lifetime scales with the experimental threshold current density in both structures, i.e.,

$$\left.\frac{J_{\mathrm{th}}^{(\mathrm{V962})}}{J_{\mathrm{th}}^{(\mathrm{V845})}}\right|_{\mathrm{exp}} \approx \left.\frac{\tau_{\mathrm{eff}}^{(\mathrm{V845})}}{\tau_{\mathrm{eff}}^{(\mathrm{V962})}}\right|_{\mathrm{sim}}. \tag{1}$$

As a result, the threshold current density of the structure increases by narrowing the injector barrier if we keep the height of the radiative barrier as high as the other barriers in the design. A multi-barrier height study presented in Ref. 19 may be a reasonable approach to improve the performance of 3P-QCLs in terms of current dynamic range and possibly output power.

The spectral measurements of this structure at different current injections and different temperatures are illustrated in Fig. 5. The lasing frequency started from 2.42 THz at the threshold and blue-shifted to 3.3 THz at an electric field before NDR at 9 K. At the current injection of 2.02 kA/cm$^2$ and higher, corresponding to a device bias of 22 V, the device lased in multiple Fabry-Perot (FP) modes that range from 2.42 THz to 3.92 THz (1.5 THz bandwidth) at 9 K. Our calculation shows that the lasing frequency changes from 2.3 THz at threshold to 3.2 THz at desired electric field of 21 kV/cm, covering most of the observed FP modes in Fig. 5. Even though our model well predicts the main lasing frequency range at different device biases, the observed high lasing frequency of 3.92 THz at high electric biases is not well explained by our RE modeling. We think that the

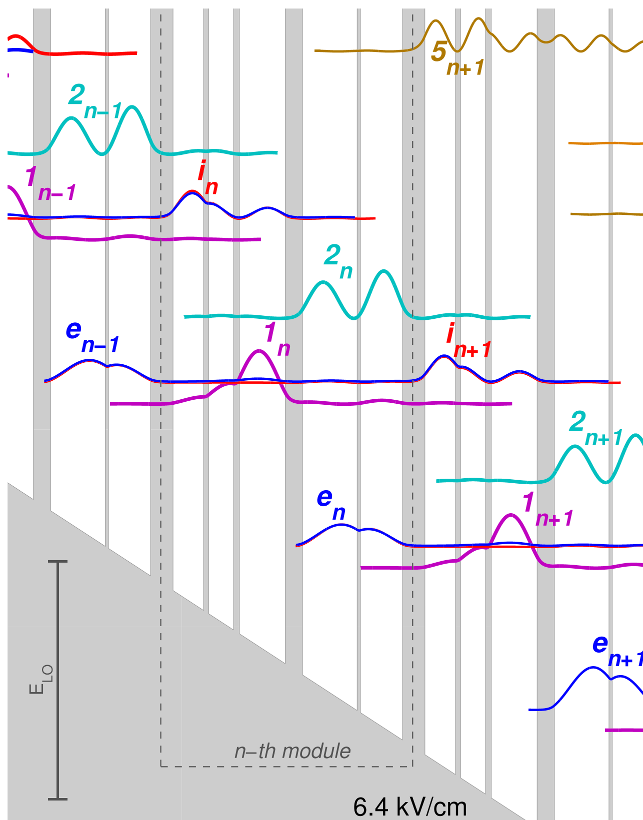


FIG. 4. Conduction band diagram and the moduli squared of wavefunctions of THz 3P-QCL at 6.4 kV/cm. States in left module (upstream), middle module, and right module (downstream) are represented by $n-1$, $n$, and $n+1$ subscripts, respectively. The extraction state ($e_{n-1}$) of each module is in resonance with state ($i_{n+1}$) of two-next module. The anticrossing energy between these states is 0.2 meV.

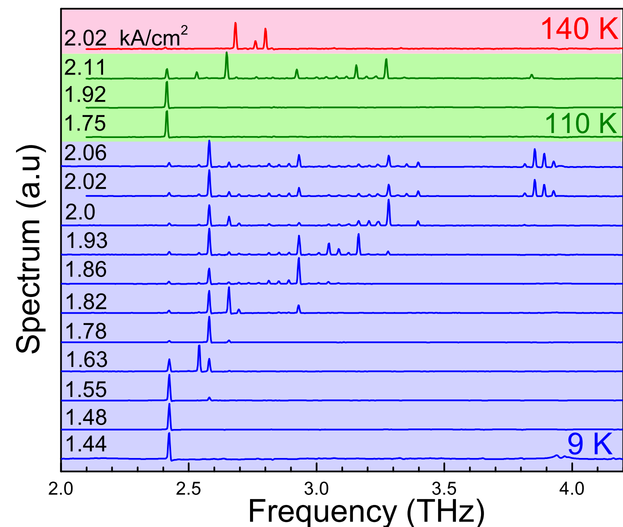


FIG. 5. THz spectra recorded for different biases and temperatures. The spectrum at 9 K and a current density higher than 2 kA/cm$^2$ shows that this IDP structure works as a wideband source.

coupling between levels $2_n$ and $6_{n+1}$ could be at play in the broad emission; for that purpose, we are currently developing a density matrix model with many states per module—like in Ref. 16—in order to understand this broad emission. This high bandwidth lasing frequency was observed even at high temperatures (up to 110 K see Fig. 5), while at 130 K and higher temperatures, 2.67 THz is the dominant FP lasing frequency.

To summarize, inserting an additional quantum-well in upstream phonon wells helped us to first, carefully engineer the wavefunctions to reduce the wrong scattering injection to the LLS ($i \rightarrow 1$) as well as the wrong tunnel injection to LLS ($e \rightarrow 1$) and second, increase the injection coupling strength by using a thinner injector barrier without increasing the risk of an early detrimental NRD before threshold. Even though the five-well design improved the performance of the 3P-QCL, this design suffered from leakage current to the higher energy states and high threshold current due to strong IR scattering. Further improvement of this scheme requires a wavefunction engineering with a specific figure of merit to minimize leakage paths to the higher states, as well as intermediate resonant current before threshold due to tunneling between both neighbouring and non-neighbouring modules. Furthermore, it becomes evident that new designs should rely on a better control—or even engineering—of interface roughness scattering.

The authors thank Andreas Wacker, Saeed Fathololoumi, and Martin Lindskog for helpful stimulating discussions. The authors would like to acknowledge the financial supports from Natural Science and Engineering Research Council (NSERC) of Canada, Canadian Foundation of Innovation (CFI), CMC Microsystems, and Ontario Research Fund (ORF).

[1]R. Kohler, A. Tredicucci, F. Beltram, H. E. Beere, E. H. Linfield, A. G. Davies, D. A. Ritchie, R. C. Iotti, and F. Rossi, Nature **417**, 156 (2002).
[2]H. Yasuda, T. Kubis, P. Vogl, N. Sekine, I. Hosako, and K. Hirakawa, Appl. Phys. Lett. **94**, 151109 (2009).
[3]T. Kubis, S. R. Mehrotra, and G. Klimeck, Appl. Phys. Lett. **97**, 261106 (2010).
[4]S. Kumar, C. W. I. Chan, Q. Hu, and J. L. Reno, Nat. Phys. **7**, 166 (2011).
[5]E. Dupont, S. Fathololoumi, Z. R. Wasilewski, G. Aers, S. R. Laframboise, M. Lindskog, S. G. Razavipour, A. Wacker, D. Ban, and H. C. Liu, J. Appl. Phys. **111**, 073111 (2012).
[6]S. Fathololoumi, E. Dupont, C. Chan, Z. Wasilewski, S. Laframboise, D. Ban, A. Mátyás, C. Jirauschek, Q. Hu, and H. C. Liu, Opt. Express **20**, 3866 (2012).
[7]S. Kumar, Q. Hu, and J. L. Reno, Appl. Phys. Lett. **94**, 131105 (2009).
[8]M. A. Belkin, J. A. Fan, S. Hormoz, F. Capasso, S. P. Khanna, M. Lachab, A. G. Davies, and E. H. Linfield, Opt. Express **16**, 3242 (2008).
[9]M. Belkin, Q. J. Wang, C. Pflugl, A. Belyanin, S. Khanna, A. Davies, E. Linfield, and F. Capasso, IEEE J. Sel. Top. Quantum Electron. **15**, 952 (2009).
[10]M. Yamanishi, K. Fujita, T. Edamura, and H. Kan, Opt. Express **16**, 20748 (2008).
[11]K. Fujita, M. Yamanishi, S. Furuta, K. Tanaka, T. Edamura, T. Kubis, and G. Klimeck, Opt. Express **20**, 20647 (2012).
[12]S. G. Razavipour, E. Dupont, S. Fathololoumi, C. W. I. Chan, M. Lindskog, Z. R. Wasilewski, G. Aers, S. R. Laframboise, A. Wacker, Q. Hu, D. Ban, and H. C. Liu, J. Appl. Phys. **113**, 203107 (2013).
[13]S. Kumar, B. S. Williams, Q. Hu, and J. L. Reno, App. Phys. Lett. **88**, 121123 (2006).
[14]M. Yamanishi, K. Fujita, S. Furuta, K. Tanaka, T. Edamura, T. Kubis, and G. Klimeck, paper presented at International Quantum Cascade Lasers School and Workshop, Baden, Austria, 2–6 September 2012.
[15]P. Patimisco, G. Scamarcio, M. V. Santacroce, V. Spagnolo, M. S. Vitiello, E. Dupont, S. R. Laframboise, S. Fathololoumi, G. S. Razavipour, and Z. Wasilewski, Opt. Express **21**, 10172 (2013).
[16]T. V. Dinh, A. Valavanis, L. J. M. Lever, Z. Ikonić, and R. W. Kelsall, Phys. Rev. B **85**, 235427 (2012).
[17]See supplementary material at http://dx.doi.org/10.1063/1.4862177 for details on scattering time between the lasing states at different electric fields.
[18]The voltage threshold of V962 is smaller than that of V845 due to the less accumulation of carriers on states *e* and *i* resulting from higher injection coupling strength.
[19]A. Mátyás, R. Chashmahcharagh, I. Kovacs, P. Lugli, K. Vijayraghavan, M. A. Belkin, and C. Jirauschek, J. Appl. Phys **111**, 103106 (2012).